Interaction of solitons with segments with modified dispersion

K. T. Stoychev, M. T. Primatarowa, and R. S. Kamburova
Institute of Solid State Physics, Bulgarian Academy of Sciences, 1784 Sofia, Bulgaria
(Received 14 February 2006; published 12 June 2006)

The interaction of nonlinear Schrödinger solitons with extended inhomogeneities with modified group-velocity (GV) and group-velocity dispersion (GVD) coefficients is investigated numerically. Increased GVD coefficients act as potential barriers and yield reflection or transmission of the incoming soliton. Decreased GVD coefficients act as potential wells, and for a given range of parameters the scattering results exhibit periodically repeating windows of trapping and transmission as a function of the length of the segment. It is shown that the escape of the soliton is due to a resonance between the period of the shape oscillations of the soliton inside the segment and the length of the latter. Segments with modified GV coefficients act as potential wells for both positive and negative values of the GV mismatch and can also lead to periodic capture-transmission scattering patterns.

DOI: 10.1103/PhysRevE.73.066611 PACS number(s): 05.45.Yv

I. INTRODUCTION

The interaction of solitons with defects and inhomogeneities is a problem of considerable interest. Scattering of nonlinear Schrödinger (NLS) solitons from point defects has been studied in [1–4] and of topological solitons in [5,6]. It has been shown in particular that kinks can be reflected by an attractive impurity via a "two-bounce" resonance mechanism involving excitation and a following deexcitation of localized impurity and shape modes. Interaction of NLS solitons with strong localized inhomogeneities in the dispersion or nonlinear coefficients has been studied in [7]. Recent investigations have been focused on the scattering of solitons from extended inhomogeneities [8–10] and nonclassical behavior has been obtained in [11,12]. Resonant interaction of NLS solitons with wide linear and nonlinear potential wells has been obtained in [13,14]. Trapping of NLS solitons in segments with inhomogeneous coupling constants has been studied in [9] within a lattice DNA model. In the present work, we investigate in detail the interaction of solitons with long (compared to the soliton's width) segments with modified group-velocity-dispersion (GVD) coefficient (Sec. II) and/or group-velocity (GV) coefficients (Sec. III) as a function of the length of the segment. While the interaction with segments with increased GVD coefficient (potential barriers) is similar to the classical-particle case, segments with decreased GVD coefficients as well as with modified GV coefficients of arbitrary sign act as potential wells and yield nonclassical evolutionary patterns, associated with the wavelike extended character of the solitons.

II. SEGMENTS WITH MODIFIED GROUP-VELOCITY-DISPERSION COEFFICIENTS

The perturbed NLS equation in the presence of a segment with modified GVD coefficient can be written as

$$i\frac{\partial\alpha}{\partial t}+M(x)\frac{\partial^2\alpha}{\partial x^2}+2|\alpha|^2\alpha=0, \tag{1}$$

where

$$M(x)=1+\mu \quad \text{for } x_1\le x\le x_2, \quad M(x)=1 \quad \text{otherwise}.$$

In an homogeneous media with $M(x)=M=\text{const}$, it possesses a fundamental bright soliton solution,

$$\alpha(x,t)=\frac{\sqrt{M}}{L}\,\text{sech}\,\frac{x-vt}{L}e^{i(vx/2M-\omega t)}, \quad \omega=\frac{v^2}{4M}-\frac{M}{L^2}, \tag{2}$$

where L and v are the width and velocity of the soliton. The energy of the soliton in this case is

$$E_s=\int_{-\infty}^{\infty}\left(M\left|\frac{\partial\alpha}{\partial x}\right|^2-|\alpha|^4\right)dx=\left(\frac{v^2}{4M}-\frac{M}{3L^2}\right)P, \tag{3}$$

where P is the norm

$$P=\int_{-\infty}^{\infty}|\alpha|^2dx=\frac{2M}{L}. \tag{4}$$

In the present work, we shall consider "slow solitons" with $v^2\ll M^2/L^2$, in which case the integrity of the solitons is preserved in the scattering process. The outcome depends in general on the interplay between E_s and the "potential energy" E_d of the interaction with the segment. The latter can be defined as

$$E_d=\mu\int_{x_1}^{x_2}\left|\frac{\partial\alpha}{\partial x}\right|^2dx. \tag{5}$$

When $|E_s|\gg|E_d|$, the solitons are not influenced significantly by the defects, and for $|E_s|\ll|E_d|$ the solitons can be reflected even by an attractive defect [1]. Below we shall study the interaction of slow solitons with extended inhomogeneities with $E_s\sim E_d$, in which case interesting resonance phenomena occur.

The energy of the soliton inside the inhomogeneity according to Eqs. (1) and (3) is

$$E_s=\left(\frac{v^2}{4(1+\mu)}-\frac{1+\mu}{3L^2}\right)P. \tag{6}$$

For small defect strengths ($|\mu|\ll1$), the loss of energy due to emitted radiation at the boundary is small and the soliton energy and the norm outside and inside the inhomogeneity

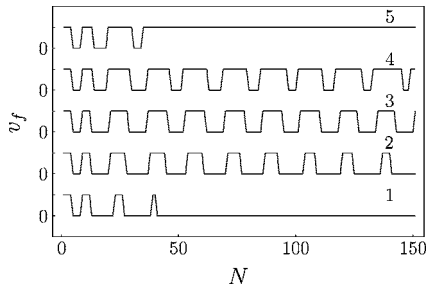

FIG. 1. Averaged final soliton velocity v_f as a function of the length N of a defect segment with $\mu=-0.3525$ for different values of the initial velocity v_0. Curves 1–5 correspond to $v_0=0.0486$, 0.0496, 0.050, 0.0504, and 0.0510, respectively. The lower horizontal parts with $v_f=0$ correspond to capture and the upper ones with $v_f>0$ to transmission. The period on curves 2–4 is $X\approx 17$.

are nearly conserved. The conservation of energy reads

$$v_0^2 - \frac{4}{3L_0^2} = \frac{v^2}{1+\mu} - \frac{4(1+\mu)}{3L^2}, \tag{7}$$

where v_0, L_0, v, and L are the soliton's velocities and widths in the ideal and defect regions, respectively. The conservation of the norm P yields

$$L = L_0(1+\mu). \tag{8}$$

The velocity of the soliton inside the segment evaluated from Eqs. (7) and (8) is

$$v^2 = (1+\mu)v_0^2 - \frac{4\mu}{3L_0^2}. \tag{9}$$

As $v_0^2 \ll 1/L_0^2$, the dependence of v on μ is governed by the last term which reflects the change of the soliton shape due to the modified GVD coefficient. Thus negative values of μ lead to an increased velocity inside the inhomogeneity, i.e., the latter acts as a potential well, while positive values of μ lead to a decrease of the velocity and act as a potential barrier.

In the numerical simulations, we employed a finite difference scheme with a fixed mesh of 2000 points in x, thus turning Eq. (1) into a set of time-dependant ordinary differential equations, which we solved using a predictor-corrector method [15]. It is known that discreteness can change the soliton's shape and velocity (see, i.e., [16]). For wide and slow solitons, however $(2L \gg 1, v \ll 1)$, these changes are negligible (they are of the order $1/6L^2$ and $v^2/6$, respectively) and the corresponding solution (2) is an excellent approximation for ideal discrete lattices (we checked its stability over long time scales). So in the numerical simulations we input the solution (2) with $2L_0=11.5$ and $v_0\approx 0.05$ as initial condition, placed 50 sites away from the defect segment. In order to eliminate boundary effects and the spurious interaction of the soliton with emitted radiation revolving along the chain, we introduced a damping term $ib(x)\alpha(x,t)$ in the equations near the turnover point $x=\pm 1000$ with $b(x)=0.1[1-(1000-|x|)/250]^2$ for $750\leq|x|\leq 1000$ and $b(x)=0$ elsewhere. Without the damping term, the norm was conserved to within 10^{-5} and the energy to within 10^{-4} for the whole course of the simulations, which proves the accuracy of the calculations.

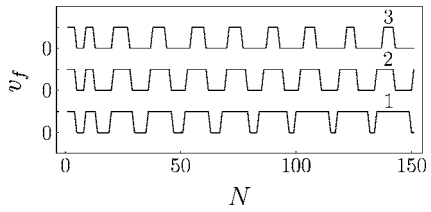

FIG. 2. Same as Fig. 1 for $v_0=0.05$ and different GVD defects. Curves 1–3 correspond to $\mu=-0.35$, -0.3525, and -0.355, respectively.

Figure 1 shows the scattering results for an attractive potential ($\mu=-0.3525$) and different values of the initial velocity v_0. Plotted is the final (averaged) soliton velocity v_f as a function of the length of the segment $N=x_2-x_1$. The lower horizontal parts with $v_f=0$ correspond to capture of the soliton inside the segment and the upper ones with $v_f>0$ to transmission. The capture-transmission patterns on curves 2–4 follow a period of ≈ 17 lattice sites. The increase of the initial velocity leads to wider region of transmission and narrower region of capture, while the total period remains nearly constant. With the increase of N, the regions of capture on curve 2 and these of transition on curve 4 become wider, at the expense of the opposite regions. The periodicity is broken on curves 1 and 5 for $N>50$. The reason for this will be explained below.

Similar plots are obtained for a fixed initial velocity v_0 and different GVD mismatch (Fig. 2). The increase of the latter yields wider regions of capture and narrower regions of transmission and vice-versa.

Three-dimensional (3D) evolutionary plots corresponding to transmission and capture are shown in Fig. 3. Sharp changes in the soliton velocity and amplitude mark the

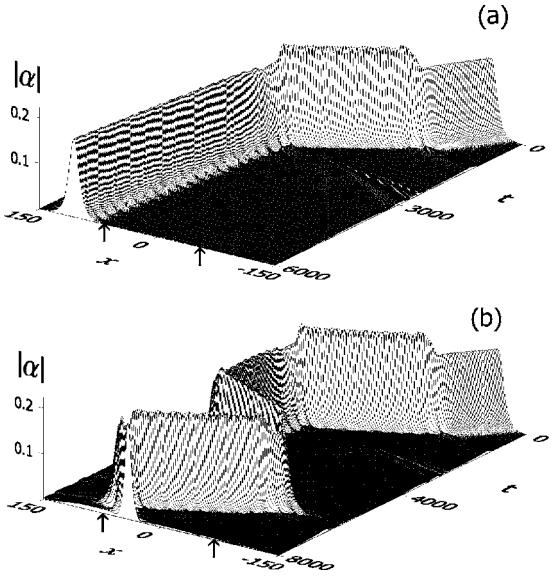

FIG. 3. 3D evolutionary plots for $v_0=0.05$ and $\mu=-0.3525$. (a) Transmission for $N=122$ and (b) capture for $N=130$. The arrows on the x axis mark the boundaries of the segment.

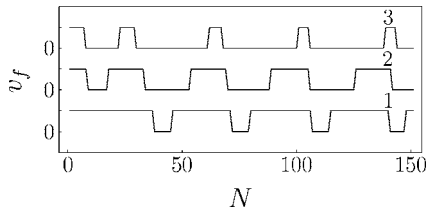

FIG. 4. Capture-transmission patterns as a function of the segment's length N for $v_0=0.05$ and different GV defects. Curves 1–3 are for $\gamma=0.08$, 0.085, and 0.09, respectively. The corresponding periods are 35, 36, and 39.

boundaries of the inhomogeneity. The velocity and the amplitude ($\sqrt{M}/L$) of the soliton increase inside the segment according to Eqs. (7) and (8) and drop when it escapes [Fig. 3(a)]. The trapping of the soliton shows a peculiar behavior [Fig. 3(b)]: it crosses the segment once, stays near the second boundary for a long time, turns back, and starts shuttling inside the segment. At the turning points, the soliton gets slightly outside the segment and its amplitude drops.

It is important to note that small-amplitude shape oscillations of the soliton are excited at the first boundary of the segment and persist for a long time. The temporal period of these oscillations inside the segment evaluated from Fig. 3 in a frame moving with the soliton is $T=137$. The velocity inside the defect region determined from Eq. (7) for $\mu=-0.35$ to -0.355 (Fig. 2) and $v_0=0.049$–0.051 (Fig. 1) is in the range $v=0.125$–0.126. Hence the spatial period of the oscillations is $X=vT\approx 17$ and coincides with the period of the capture-transmission patterns in Figs. 1 and 2. This shows unambiguously that the periodicity is due to a resonance between the length of the inhomogeneity and the spatial period of the shape oscillations excited at the boundary, or equivalently, the time for which the soliton crosses the inhomogeneity and the temporal period of the shape oscillations.

Shape oscillations of perturbed NLS solitons have been studied using the inverse-scattering transform (IST) [17–20], small-amplitude linear wave expansion around the soliton solution [22,21], or the collective-coordinate (variational) approach [20,23,24]. Within the second method, the solution of the perturbed NLS equation can be represented in the form

$$\alpha(x,t)=\{\varphi_0(x,t)+\varphi_1(x,t)e^{-i\omega_1 t}+\varphi_2^*(x,t)e^{i\omega_1 t}\}e^{i(vx/2M-\omega_0 t)}, \tag{10}$$

where φ_0 is the envelope of the unperturbed solution (2) and the functions φ_1 and φ_2 describe the small-amplitude perturbation. They satisfy the linear system of equations,

$$\frac{\partial^2\varphi_1}{\partial x^2}+\left(4\varphi_0^2-\frac{M}{L^2}+\omega_1\right)\varphi_1+2\varphi_0^2\varphi_2=0$$

$$\frac{\partial^2\varphi_2}{\partial x^2}+\left(4\varphi_0^2-\frac{M}{L^2}-\omega_1\right)\varphi_2+2\varphi_0^2\varphi_1=0. \tag{11}$$

The spectrum of Eqs. (11) consists of a discrete eigenvalue $\omega_1=0$ corresponding to a static perturbation of the soliton, and a band of frequencies $\omega_1=(M/L^2+\kappa^2)$ [22] describing the shape modes. The frequency of the shape oscillations in Fig. 3 is $\omega=2\pi/T=0.0458$ and coincides with the band-edge frequency of the shape modes ($\omega=M/L^2=0.0465, \kappa=0$). The corresponding solution of Eqs. (11) is

$$\varphi_1(\xi)=a_0\tanh^2\frac{x-vt}{L}, \quad \varphi_2(\xi)=-a_0\mathrm{sech}^2\frac{x-vt}{L}, \tag{12}$$

where $a_0\ll 1/L$. Shape oscillations of perturbed NLS solitons with frequency $\omega=M/L^2$ emerge also within the inverse-scattering transform as a result of interference with emitted radiation. The collective coordinate approach yields a lower shape mode frequency $(2/\pi)M/L^2$, and it has been argued that it is not appropriate for single-soliton interactions [20] and multiple scattering [9].

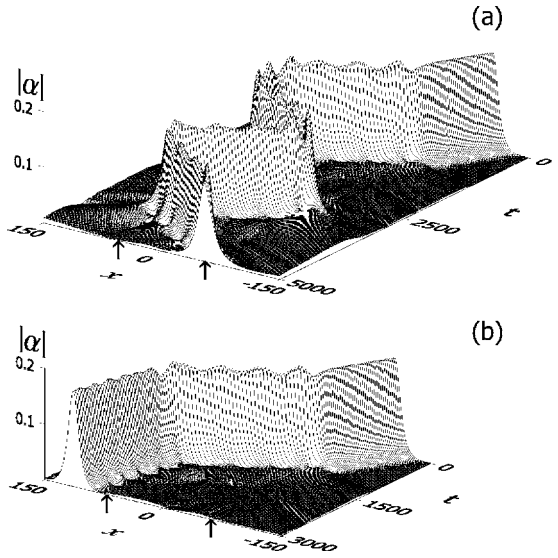

FIG. 5. 3D evolutionary patterns for $v_0=0.05$ and $\gamma=0.085$. (a) Capture ($N=110$) and (b) transmission ($N=130$).

The periodic evolutionary patterns in Figs. 1 and 2 can be explained qualitatively in the following way: when the incoming soliton reaches the boundary of the segment, it interacts inelastically with it and loses part of its energy exciting small-amplitude shape oscillations. These oscillations are weakly decaying and persist for a long time. When the oscillating soliton reaches the second boundary, different outcomes are possible depending on the phase. In the nonresonant case, the reduced energy of the soliton does not allow it to overcome the potential barrier of the second boundary; it is reflected from it and eventually gets trapped. However, whenever the time for which the soliton crosses the potential well is commensurate with the period of the shape oscillations, the inelastic interaction with the second boundary may extinguish the shape oscillations, restoring the soliton energy and allowing it to overcome the barrier and escape. The higher the initial velocity of the soliton, the wider the escape regions as seen from Fig. 1. The broken periodicity on curves 1 and 5 is due to the decay of the shape mode due to emission of radiation. Thus for very wide segments, the periodicity vanishes and the soliton is either transmitted or trapped

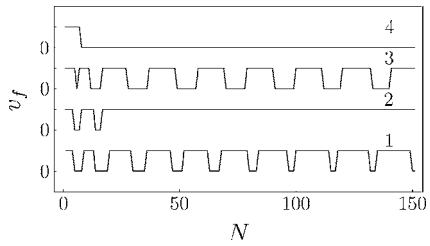

FIG. 6. Regions of capture and transmission as a function of N for segments with $\mu=-0.3525$ and different GV-defect coefficients. Curves 1–4 correspond to $\gamma=0.0$, 0.025, 0.05, and 0.07, respectively.

depending on whether its final kinetic energy is above or below the potential barrier of the second boundary.

The escape mechanism described above is not obvious from the 3D plots in Fig. 3(a), as the shape oscillations persist outside the inhomogeneity too. However, a closer inspection of the period of the oscillations outside the segment reveals a period of $T=207$, which coincides with the soliton period in the ideal part of the lattice. Thus the resonant inelastic interaction of the oscillating soliton with the second boundary is a complex (two-step) process: the shape oscillations with period $T=137$ are extinguished, which allows the soliton to escape, and new oscillations with $T=207$ are excited immediately.

An increase of the depth of the potential leads to wider regions of trapping and narrower regions of transmission (Fig. 2, curves 1–3). The perturbation that the boundary induces is stronger in this case, and a larger portion of the soliton energy is transformed into a shape mode. Hence a more exact resonance condition is required at the second boundary for escape, which yields narrower escape regions.

III. SEGMENTS WITH MODIFIED GROUP-VELOCITY AND GROUP-VELOCITY-DISPERSION COEFFICIENTS

The perturbed NLS equation in the presence of a segment with modified GV and GVD coefficients is

$$i\frac{\partial\alpha}{\partial t}+i\gamma(x)\frac{\partial\alpha}{\partial x}+M(x)\frac{\partial^2\alpha}{\partial x^2}+2|\alpha|^2\alpha=0, \tag{13}$$

$$\gamma(x)=\gamma, M(x)=1+\mu \quad \text{for } x_1\le x\le x_2, \quad \gamma(x)=0,$$

$$M(x)=1 \quad \text{otherwise},$$

where γ is the GV defect. Equation (13) with constant γ and M governs the dynamics of circularly polarized solitons in gyrotropic media [25,26] and of linearly polarized solitons in birefringent fibers. For a homogeneous media with $\gamma=$const and $M=$const, it possesses the following one-soliton solution:

$$\alpha(x,t)=\frac{\sqrt{M}}{L}\,\mathrm{sech}\,\frac{x-vt}{L}e^{i[(v/2+\gamma)x/M-\omega t]}, \tag{14}$$

$$\omega=\frac{v^2}{4M}-\frac{\gamma^2}{M}-\frac{M}{L^2}.$$

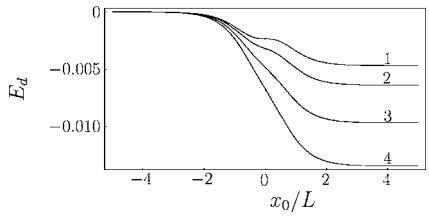

FIG. 7. Scattering potential profiles near the boundary of a defect segment ($x_0>0$). x_0 is the distance from the center of the soliton to the boundary and L is the width of the soliton. Curves 1–4 correspond to curves 1–4 in Fig. 6.

The soliton energy in this case is

$$E_s=\int_{-\infty}^{\infty}\left[M\left|\frac{\partial\alpha}{\partial x}\right|^2+i\gamma\left(\alpha^*\frac{\partial\alpha}{\partial x}-\alpha\frac{\partial\alpha^*}{\partial x}\right)-|\alpha|^4\right]dx$$

$$=\left(\frac{v^2}{4M}-\frac{M}{3L^2}-\frac{\gamma^2}{M}\right)P, \tag{15}$$

where the norm P is given by Eq. (4) and does not depend on γ.

The energy balance outside and inside the inhomogeneity yields

$$v_0^2-\frac{4}{3L_0^2}=\frac{v^2}{1+\mu}-\frac{4(1+\mu)}{3L^2}-\frac{4\gamma^2}{1+\mu}, \tag{16}$$

where we have neglected the small energy loss at the boundary. Using the norm-conservation condition (8), we obtain

$$v^2=(1+\mu)v_0^2-\frac{4\mu}{3L_0^2}+4\gamma^2. \tag{17}$$

For a purely gyrotropic defect segment ($\mu=0$) this gives

$$v^2=v_0^2+4\gamma^2. \tag{18}$$

This is an important and somewhat unexpected result, showing that the velocity of the soliton inside a GV inhomogeneity increases, independently of the sign of the GV mismatch, i.e., such an inhomogeneity always acts on the soliton as a potential well. In all other perturbations we have studied so far (linear, nonlinear, and GVD), the sign of the perturbation determines the sign of the potential "seen" by the soliton.

Applied to circularly polarized solitons with opposite handedness (opposite signs of γ) entering a gyrotropic segment, it follows from Eq. (18) that their velocities will be

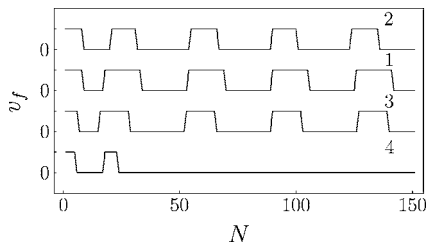

FIG. 8. Regions of capture and transmission as a function of N for $v_0=0.05$, $\gamma=0.085$, and different GVD defects. Curves 1–4 correspond to $\mu=0.0$, −0.1, 0.25, and 0.35, respectively.

equal, while their carrier wave numbers will be modified according to Eq. (14) as $k_{\pm}=(v/2\pm\gamma)/M$, and so will be their phase velocities $\omega/k_{\pm}$. Thus a linearly polarized pulse (formed of two conjugate circularly polarized pulses) entering a gyrotropic segment will keep its shape, increase its velocity, and have a rotating plane of polarization. Its scattering patterns will be the same as these of the circularly polarized pulses.

Figure 4 shows schematically the dependence of the scattering results on the length of a GV-defect segment. Periodically repeating windows of capture and transmission are observed, similarly to the case of a segment with modified GVD coefficient. The increase of the GV coefficient leads to wider windows of capture and narrower windows of transmission, and vice versa. 3D evolutionary plots corresponding to transmission and capture are shown in Fig. 5. The spatial period of the shape oscillations 36 is in excellent agreement with the corresponding capture-transmission period in Fig. 4, curve 2.

The combined effect of a segment with a strong GVD and a weak GV mismatch is shown in Fig. 6. Curve 1 corresponds to the pure GVD case. The addition of a weak GV defect (Fig. 6, curve 2) removes the periodicity and leads to transmission for segments with $N>22$. This is a peculiar behavior, as both potentials are attractive and one can expect that their overlapping should favor capture of the solitons. An increase of the GV coefficient reintroduces the periodic capture-transmission pattern (Fig. 6, curve 3), and a further increase leads to capture of the solitons for $N>15$ (Fig. 6, curve 4). The explanation of the observed peculiarities is the following: the energy stored into the shape mode depends on the perturbation of the soliton at the boundary, which is related to the profile of the potential. Slowly varying potentials induce weaker perturbations, while potentials with more steep and more complex profiles induce stronger perturbations. Near the boundary of a long segment, the scattering potential is given by

$$E_d=\int_{-\infty}^{x_0}\left\{\mu\left|\frac{\partial\alpha}{\partial x}\right|^2+i\gamma\left(\alpha^*\frac{\partial\alpha}{\partial x}-\alpha\frac{\partial\alpha^*}{\partial x}\right)\right\}dx, \quad (19)$$

where x_0 is the distance from the center of the soliton to the boundary. The potential profiles near the boundaries of segments with modified GVD and GV coefficients corresponding to Fig. 6 are shown in Fig. 7. Note that the profile for the purely GVD defect (Fig. 7, curve 1) has a step in the middle, which seems to increase the perturbation at the boundary. Adding a small GV mismatch (Fig. 7, curve 2) smooths out the GVD potential step and decreases the perturbation, leading to escape of the soliton, although the combined potential well has become deeper. A further increase of the GV coefficient (Fig. 7, curves 3 and 4) makes the resulting potential well considerably deeper and with a steeper profile, and although without a step, the latter increases the perturbation and eventually leads to capture.

The scattering results for the opposite case, corresponding to a small GVD defect added to a GV defect segment, is shown in Fig. 8. For a negative GVD defect (attraction), the regions of capture become wider (Fig. 8, curve 2) as can be expected. A peculiar behavior here is observed in curves 3 and 4, where *positive* values of the GVD defect (repulsive potential) lead again to an increase of the regions of capture, although the resulting potential well has become shallower. This can be associated with the more complex potential profiles (Fig. 9, curves 3 and 4), which apparently induce stronger perturbations. It is worth mentioning that a further increase of the positive GVD mismatch did not lead to regions of transmission, as could be expected, but eventually lead to reflection of the soliton from the first boundary.

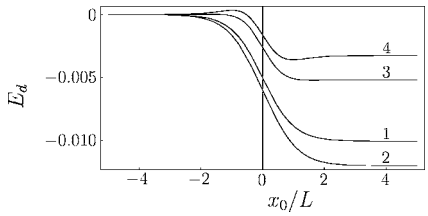

FIG. 9. Scattering potential profiles near the boundary, corresponding to curves 1–4 in Fig. 8.

IV. SUMMARY

We have investigated numerically the interaction of NLS solitons with long (compared to the soliton width) segments with modified group-velocity and group-velocity-dispersion coefficients. Decreased GVD coefficients act as potential wells and for a given range of parameters yield periodically repeating regions of transmission or capture of the solitons as a function of the length of the segment. It is shown that this phenomenon is due to a resonance between the period of the shape oscillations of the soliton, excited at the first boundary (which take away part of the soliton energy) and the length of the segment. In the nonresonant case, the reduced kinetic energy of the soliton is not sufficient for it to overcome the potential barrier of the second boundary and it gets trapped. When the length of the segment is commensurate with the spatial period of the shape oscillations of the soliton, the inelastic interaction with the second boundary may extinguish the shape mode, transferring its energy back into kinetic energy of the soliton and allowing it to escape.

A GV-defect segment introduces an attractive potential well for both positive and negative signs of the GV mismatch and for a certain range of parameters yields similar periodic capture-transmission patterns. The combination of GV and GVD-defect segments shows some peculiarities, i.e., a nonmonotonous behavior with the increase of one of the coefficients. This is explained by the different shapes of the corresponding potentials and the fact that the GVD defect has a more complicated potential profile which yields stronger perturbation on the soliton.

ACKNOWLEDGMENTS

This work is supported in part by the National Science Foundation of Bulgaria under Grant No. F1414.

[1] Yu. S. Kivshar, A. M. Kosevich, and O. A. Chubykalo, Zh. Eksp. Teor. Fiz. **93**, 968 (1987) [Sov. Phys. JETP, **66**, 545 (1987)]; Phys. Lett. A **125**, 35 (1987).
[2] D. I. Pushkarov and R. D. Atanasov, Phys. Lett. A **149**, 287 (1990).
[3] X. D. Cao and B. A. Malomed, Phys. Lett. A **206**, 177 (1995).
[4] V. V. Konotop, D. Cai, M. Salerno, A. R. Bishop, and N. Grønbech-Jensen, Phys. Rev. E **53**, 6476 (1996).
[5] Yu. S. Kivshar, Zhang Fei, and L. Vázquez, Phys. Rev. Lett. **67**, 1177 (1991).
[6] Zhang Fei, Yu. S. Kivshar, and L. Vázquez, Phys. Rev. A **45**, 6019 (1992); **46**, 5214 (1992).
[7] S. Burtsev, D. J. Kaup, and B. A. Malomed, Phys. Rev. E **52**, 4474 (1995).
[8] R. Scharf and A. R. Bishop, Phys. Rev. A **46**, R2973 (1992).
[9] J. J.-L. Ting and M. Peyrard, Phys. Rev. E **53**, 1011 (1996).
[10] H. Frauenkron and P. Grassberger, Phys. Rev. E **53**, 2823 (1996).
[11] G. Kälbermann, Phys. Lett. A **252**, 37 (1999); Chaos, Solitons Fractals **12**, 625 (2001); **12**, 2381 (2001).
[12] Y. Nogami and F. M. Toyama, Phys. Lett. A **184**, 245 (1994).
[13] K. T. Stoychev, M. T. Primatarowa, and R. S. Kamburova, Phys. Rev. E **70**, 066622 (2004).
[14] M. T. Primatarowa, K. T. Stoychev, and R. S. Kamburova, Phys. Rev. E **72**, 036608 (2005).
[15] L. F. Shampine and M. K. Gordon, *Computer Solution of Ordinary Differential Equations* (Freeman, San Francisco, 1975).
[16] L. N. Trefethen, SIAM Rev. **24**, 113 (1982).
[17] J. Satsuma and N. Yajima, Suppl. Prog. Theor. Phys. **55**, 284 (1974).
[18] J. P. Gordon, J. Opt. Soc. Am. B **9**, 91 (1992).
[19] M. W. Chbat, J. P. Prucnal, M. N. Islam, C. E. Soccolich, and J. P. Gordon, J. Opt. Soc. Am. B **10**, 1386 (1993).
[20] E. A. Kuznetsov, A. V. Mikhailov, and I. A. Shimokhin, Physica D **87**, 201 (1995).
[21] Y. S. Kivshar, D. E. Pelinovsky, T. Cretegny, and M. Peyrard, Phys. Rev. Lett. **80**, 5032 (1998).
[22] D. J. Kaup, Phys. Rev. A **42**, 5689 (1990).
[23] T. Ueda and W. L. Kath, Phys. Rev. A **42**, 563 (1990).
[24] B. A. Malomed and R. S. Tasgal, Phys. Rev. E **58**, 2564 (1998).
[25] M. T. Primatarowa and K. T. Stoychev, Phys. Rev. B **49**, 6634 (1994).
[26] K. T. Stoychev, M. T. Primatarowa, and R. S. Kamburova, J. Phys.: Condens. Matter **12**, 10429 (2000).